Original Research

AQP9 in Neutrophils Promotes the Formation of NETs by Regulating JAK2-STAT3 Pathway-Mediated Pyroptosis to Aggravate Intestinal Epithelial Cell Injury in Ulcerative Colitis

Zetao Wang[1,2,3,†], Yao Sun[1,2,†], Xiaohui Zhou[1,2], Jianing Shi[4], Lijun Shi[1,2,*] ⓘ

[1]Department of Gastroenterology, The First Affiliated Hospital of Harbin Medical University, 150006 Harbin, Heilongjiang, China
[2]Key Laboratory of Hepatosplenic Surgery, Ministry of Education, The First Affiliated Hospital of Harbin Medical University, 150006 Harbin, Heilongjiang, China
[3]Fifth Department of Medicine (Nephrology/Endocrinology/Rheumatology, Pneumonology), University Medical Center Mannheim, University of Heidelberg, 69117 Mannheim, Baden-Wurttemberg, Germany
[4]Endoscopy Center, Department of Gastroenterology, Shanghai East Hospital, School of Medicine, Tongji University, 200092 Shanghai, China
*Correspondence: 1433@hrbmu.edu.cn (Lijun Shi)
[†]These authors contributed equally.

Abstract

Background: Ulcerative colitis (UC) is a chronic inflammatory disorder primarily affecting the rectum and colon. This study aimed to identify potential therapeutic targets that may inhibit UC progression and mitigate patient suffering. **Methods**: UC-related datasets were retrieved from the Gene Expression Omnibus database. Differential expression analysis, weighted gene co-expression network analysis, immunoinfiltration analysis, and pyroptosis scoring were employed to identify key pyroptosis-related genes implicated in UC pathogenesis. A dextran sulfate sodium salt (DSS)-induced mouse model of UC was established, and neutrophil extracellular traps (NETs) were induced in neutrophils by stimulation with phorbol 12-myristate 13-acetate (PMA). Histopathological changes in mouse colon tissues were assessed by hematoxylin-eosin staining, and NET formation was evaluated via immunofluorescence. The expression of aquaporin 9 (AQP9), peptidylarginine deiminase 4 (PAD4), zonula occludens 1 (ZO-1), occludin, and proteins related to pyroptosis and the JAK2-STAT3 pathway was determined by Western blotting. Levels of inflammatory cytokines were measured by enzyme-linked immunosorbent assay (ELISA), production of reactive oxygen species was assessed using fluorescent probes, and intestinal epithelial cell viability and death were evaluated using the cell counting kit-8 (CCK-8) and terminal deoxynucleotidyl transferase dUTP nick end labeling (TUNEL) assays, respectively. **Results**: Five hub genes (*AQP9*, *S100A8*, *S100A9*, *S100A12*, and *VNN2*) were identified through bioinformatics analysis, with AQP9 selected for further investigation. Single-cell analysis and immunofluorescence revealed that AQP9 was predominantly expressed in neutrophils and upregulated in the colon tissues of mice with UC and PMA-stimulated neutrophils. Knockdown of AQP9 in PMA-treated neutrophils led to suppression of the JAK2-STAT3 pathway, reduced pyroptosis, and decreased NET formation. Upon co-culture with intestinal epithelial cells, AQP9 knockdown resulted in enhanced epithelial cell viability, reduced apoptosis, and upregulation of ZO-1 and occludin. Conversely, treatment of neutrophils from the PMA+si-AQP9 with a JAK2-STAT3 pathway agonist increased pyroptosis, enhanced the formation of NETs, and induced epithelial cell injury. Similarly, treatment with a pyroptosis agonist enhanced both pyroptosis and the formation of NETs, further aggravating epithelial damage. **Conclusion**: Knockdown of AQP9 inhibits JAK2-STAT3 pathway-mediated pyroptosis, thereby reducing the formation of NETs and attenuating intestinal epithelial cell injury.

Keywords: colitis; pyroptosis; neutrophil; extracellular traps

1. Introduction

Ulcerative colitis (UC) is a recurrent and remitting inflammatory bowel disease (IBD) [1]. It is frequently characterized by intestinal mucosal epithelial injury and disruption of intestinal homeostasis. Clinically, patients with UC present with symptoms including abdominal pain, hematochezia, fatigue, and fecal incontinence [2]. In recent years, the incidence of UC has been steadily increasing, which has contributed to a parallel rise in the prevalence of colorectal cancer. Currently, pharmacological therapy, often in combination with colectomy, constitutes the mainstay

of UC management [3,4]. However, the use of therapeutic agents is frequently associated with adverse effects. For instance, 5-aminosalicylic acid has been reported to induce high-grade fever and severe allergic reactions, and corticosteroids have been linked to reduced bone mineral density, an elevated risk of fractures and infections, as well as hepatotoxicity and nephrotoxicity [5]. Moreover, the complex pathophysiology of UC, compounded by inter-individual variability, often limits the efficacy of conventional pharmacotherapy. Consequently, growing attention has been directed toward the development of targeted therapies for UC.

Publisher's Note: IMR Press stays neutral with regard to jurisdictional claims in published maps and institutional affiliations.

Such approaches are increasingly guided by cytokine profiles associated with disease stage and patient-specific expression patterns [6]. Identifying novel therapeutic targets is therefore an essential step toward improving the safety and effectiveness of UC treatment.

Neutrophils, as short-lived effector cells of the innate immune system, play a paradoxical and context-dependent role in acute inflammation [7]. In response to microbial invasion or inflammatory stimuli, neutrophils migrate to sites of mucosal injury. At these sites, they contribute to host defense by releasing reactive oxygen species (ROS) and forming neutrophil extracellular traps (NETs), which together facilitate the clearance of intestinal pathogens [7]. Nonetheless, excessive neutrophil activation can aggravate tissue injury, disrupt intestinal homeostasis, and elevate the risk of thrombosis [8,9]. In recent years, NETs have attracted increasing attention for their involvement in various diseases, including arteriosclerosis, cancer, and immune-mediated diseases. In UC, Vincenzo Dinallo *et al*. [10] reported that mucosal injury generally occurs in regions infiltrated by neutrophils, and NETs are primarily localized within mucosal areas of active inflammation. Therefore, NETs maintain the inflammatory signal of UC.

Pyroptosis is a form of programmed cell death that not only affects the rupture of the plasma membrane of neutrophils but also plays an important role in the release of NETs [11]. Therefore, this study aimed to identify pyroptosis-related genes that may affect the progression of UC and regulate the formation of NETs via bioinformatics analysis.

2. Materials and Methods

2.1 Data Acquisition and Processing

Raw count data were retrieved from the GSE193677 and GSE214695 datasets available in the Gene Expression Omnibus database (http://www.ncbi.nlm.nih.gov/geo/). The GSE193677 dataset includes 872 UC and 461 Control samples, whereas the GSE214695 dataset consists of 6 UC and 6 Control samples. Ensembl IDs in both datasets were converted to gene symbols using the reference genome hg19. The count expression matrices were subsequently processed using the "edgeR" package (v 3.40.1) in R (v 4.2.2, R Foundation for Statistical Computing, Vienna, Austria) to compute average values and normalize expression levels for genes with multiple entries.

2.2 Differential Expression Analysis and Functional Enrichment Analysis

The "edgeR" package was employed for screening differentially expressed genes (DEGs), with the screening criteria set as $|\log_2 FC| > 1$ & adj. *p* value < 0.05. Gene ID conversion was performed on the identified DEGs using "org.Hs.eg.db", and functional enrichment analysis was conducted using the "clusterProfiler" package (v 4.4.4).

2.3 Single-Cell Analysis

Single-cell analysis was carried out using the "Seurat" package (v 4.3.0.1). Cells were screened based on the criteria of $200 < nFeature RNA < 6000$. Cell type annotation was subsequently conducted using the SingleR package (v 2.2.0).

2.4 Pyroptosis Analysis

Pyroptosis-related genes were obtained through a systematic literature review [12]. Differential expression analysis of these genes was performed using the GSE193677 dataset. Heatmaps were plotted using the "pheatmap" package. Gene set variation analysis (GSVA) was carried out using the "GSVA" package to calculate pyroptosis scores for each sample group.

2.5 Weighted Gene Co-Expression Network Analysis (WGCNA)

The "WGCNA" package (v 1.71) was applied for conducting WGCNA on the identified key genes, and the "clusterProfiler" package was employed for performing Kyoto Encyclopedia of Genes and Genomes (KEGG) and Gene Ontology (GO) enrichment analyses.

2.6 Hub Gene Screening

The STRING database (https://string-db.org/, v 11.5) was used for carrying out protein-protein interaction (PPI) analysis. The MCODE plug-in in Cytoscape (v 3.9.1) was employed to identify key genes within the PPI networks. Hub gene screening was performed using the following three machine learning approaches: LASSO regression using the "glmnet" package (v 4.1-4), random forest analysis using the "randomForest" package (v 4.7-1.1), and support vector machine-recursive feature elimination (SVM-RFE) using the "CARET" (v 6.0-92) and "e1071" (v 1.7-11) packages. Venn diagrams were generated with the "Venn" package. Single-sample gene set enrichment analysis (ss-GSEA) of aquaporin 9 (AQP9) was performed using GSEA (v 4.3.2).

2.7 Immunoinfiltration Analysis

Immune cell infiltration analysis was performed on normalized expression data using the "CIBERSORT" package (v 1.04). Bar plots were generated to visualize the relative proportions of immune cells. Correlation analysis among immune cell types was conducted using the "corrplot" package (v 0.92), with scatter plots and boxplots created using the "ggplot2" and "ggpubr" (v 0.6) packages.

2.8 Animal Grouping and Model Establishment

Male C57BL/6 mice (SPF, 6–8 weeks old) were obtained from Beijing Vital River Laboratory Animal Technology Co., Ltd., and housed in an 18–22 °C facility with ad libitum access to water and food. Following a one-week acclimatization period, twelve mice were randomly assigned

to two groups: Control (n = 6) and UC (n = 6). Mice in the UC group were continuously administered with drinking water containing 2% (w/v) dextran sulfate sodium salt (DSS) (Sigma, Shanghai, China, 265152-M) for 7 days, while mice in the Control group were fed with normal drinking water. Predefined humane endpoints were established such that mice exhibiting signs of severe pain during the experiment would be euthanized prior to the study completion. However, none of the mice were euthanized, and all mice survived until the end of the experiment. After 7 days of treatment as described above, mice were euthanized for colon tissue collection to evaluate whether the model was successfully constructed. Euthanasia was performed using CO_2 inhalation at a controlled replacement rate of 30%–70% of the container volume/minute to ensure rapid and humane loss of consciousness. This experiment was approved by the Ethics Committee of Laboratory Animal Management and Welfare of the First Affiliated Hospital of Harbin Medical University (Approval No.: IACUC-2023053), and was conducted following the ARRIVE guidelines.

2.9 Cell Culture and Model Construction

Human neutrophils (Immocell, Xiamen, Fujian, China, IMP-H209) and human intestinal epithelial cells (YaJi Biological, Shanghai, China, YS3102C) were utilized in this study. Neutrophils were cultured in a specialized medium (Immocell, Xiamen, Fujian, China, IMP-H209-1), while intestinal epithelial cells were maintained in Opti-MEM medium supplemented with fetal bovine serum (ThermoFisher, Shanghai, China, A5256701), EGF, and GlutaMAX™ (ThermoFisher, Shanghai, China, 42360032). Cells were cultured under standard conditions (37 °C, 5% CO_2). Formation of NETs was induced by stimulating neutrophils with 100 nM/L phorbol 12-myristate 13-acetate (PMA) for 4 h. Cells were transfected with either the constructed AQP9-targeting siRNA or si-NC. Pyroptosis was induced by treating the cells with 10 μM nigericin for 24 h. Activation of the JAK2-STAT3 pathway was achieved by exposing the cells to 20 μM Colivelin for 12 h. All cell lines were validated by STR profiling and tested negative for mycoplasma.

2.10 Hematoxylin-Eosin (HE) Staining

Tissue samples were fixed in 4% paraformaldehyde, embedded in paraffin, and sectioned into 4 μm slices. Sections were stained with HE (Beyotime, Shanghai, China, C0105S) and examined microscopically.

2.11 Immunofluorescence

1×10^6 cells were inoculated into 24 mm sterile cell slides and placed in 6-well plates. the following adherence, cells were fixed with 4% paraformaldehyde and blocked using a blocking buffer. Cells were then incubated sequentially with primary and secondary antibodies, followed by nuclear staining with DAPI. Slides were mounted and visualized under a microscope. Primary antibodies used were myeloperoxidase (MPO, Cell Signaling Technology, Danvers, MA, USA, 14569) and citrullinated histone H3 (CitH3, Cell Signaling Technology, Danvers, MA, USA, 97272).

2.12 Western Blotting (WB)

Total protein was extracted from colon tissues or cultured cells using a lysis buffer containing 1% protease inhibitor, and then quantified using the BCA kit (Beyotime, Shanghai, China, P0012S). Electrophoresis, membrane transfer, antibody incubation, and color development were subsequently performed. The antibodies used included cleaved N-terminal gasdermin D (GSDMD-N, Cell Signaling Technology, Danvers, MA, USA, 36425), GS-DMD (Cell Signaling Technology, Danvers, MA, USA, 39754), p-STAT3 (Cell Signaling Technology, Danvers, MA, USA, 9145), p-JAK2 (Cell Signaling Technology, Danvers, MA, USA, 3776), JAK2 (Cell Signaling Technology, Danvers, MA, USA, 3230), STAT3 (Cell Signaling Technology, Danvers, MA, USA, 12640), AQP9 (Invitrogen, Shanghai, China, PA5-114872), ZO-1 (Invitrogen, Shanghai, China, 61-7300), and occludin (Cell Signaling Technology, Danvers, MA, USA, 91131). β-actin (Cell Signaling Technology, Danvers, MA, USA, 4970S) was set as the internal reference protein.

Table 1. Primer sequences.

Primer	Primer sequences
mmu-AQP9-F	5′-CGGATGAAGGGACAAGGTAGCC-3′
mmu-AQP9-R	5′-ACAGAGAGCCACTAAGGAAGAAAGG-3′
mmu-GAPDH-F	5′-GATCATCAGCAATGCCTCCT-3′
mmu-GAPDH-R	5′-TGTGGTCATGAGTCCTTCCA-3′

AQP9, aquaporin 9; GAPDH, glyceraldehyde-3-phosphate dehydrogenase.

2.13 Enzyme-Linked Immunosorbent Assay (ELISA)

The expression levels of corresponding inflammatory factors were measured using the following ELISA kits: mouse interleukin (IL)-1β (Beyotime, Shanghai, China, PI301), mouse IL-18 (Beyotime, Shanghai, China, PI553), human IL-1β (Beyotime, Shanghai, China, PI305), human IL-18 (Beyotime, Shanghai, China, PI558), and MPO-DNA (COIBO BIO, Shanghai, China, CB21448-Hu).

2.14 qRT-PCR

Total RNA was extracted from colon tissues using the TRIzol reagent. RNA purity and integrity were assessed via agarose gel electrophoresis, and the A260/A280 ratio was measured by NanoDrop 2000 spectrophotometry. cDNA synthesis was performed using the PrimeScript RT kit (TaKaRa, Beijing, China, RR014A). qRT-PCR was conducted with PowerTrack™ SYBR Green Master Mix
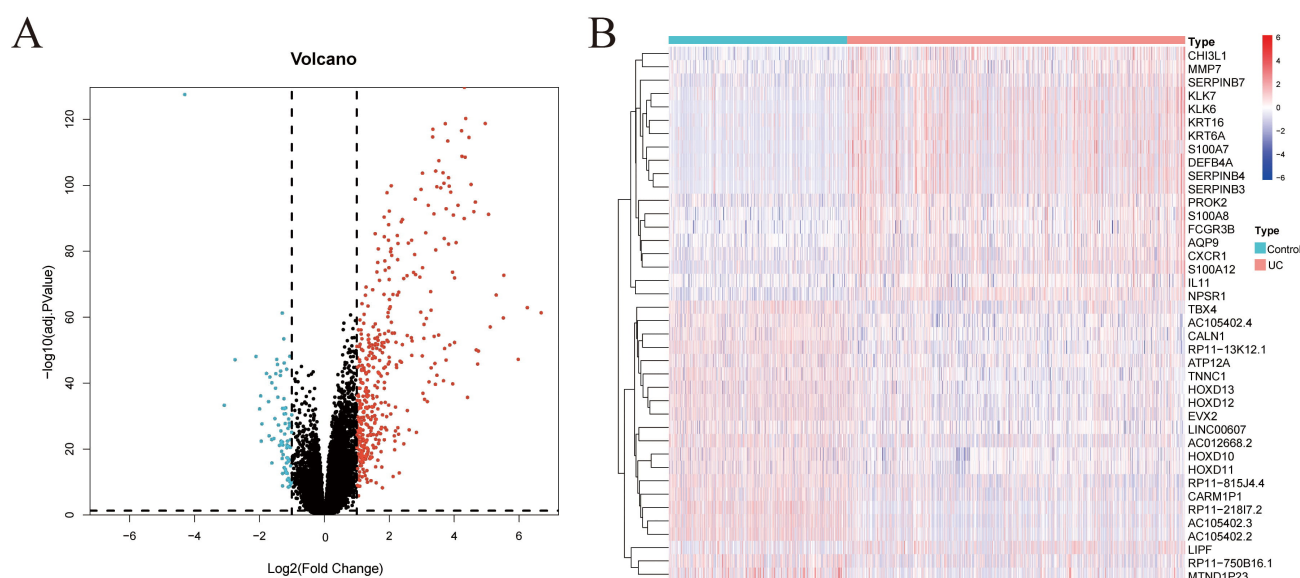
Fig. 1. Screening of DEGs. (A) Volcano map showing the results of differential expression analysis from the GSE193677 dataset. (B) Heatmap showing the expression of DEGs across samples from different groups in the GSE193677 dataset. DEGs, differentially expressed genes.

(Applied Biosystems, Shanghai, China, A46012) as per the manufacturer's instructions. Primer sequences are listed in Table 1. The relative expression of mRNA was calculated using the $2^{-\Delta\Delta Ct}$ method.

2.15 Cell Counting Kit-8 (CCK-8) Assay

CCK-8 assay was carried out according to the manufacturer's manual (Beyotime, Shanghai, China, C0037). A total of 2000 cells were added to each well of the 96-well plate and incubated for 24 h. Subsequently, 10 μL of the CCK-8 solution was added to each well, and incubation was performed at 37 °C for 2 h. Absorbance at 450 nm was measured using a microplate reader.

2.16 Terminal Deoxynucleotidyl Transferase dUTP Nick end Labeling (TUNEL) Assay

Cell death was detected using a TUNEL assay kit (Beyotime, Shanghai, China, C1086). Briefly, cells were fixed with 4% paraformaldehyde for 30 min, and incubated with PBS containing 0.3% Triton X-100, at room temperature for 5 min. Subsequently, cells were incubated with 50 μL of TUNEL reaction mixture at 37 °C for 60 min. After mounting with an anti-fade sealing solution, samples were analyzed via fluorescence microscopy.

2.17 Measurement of ROS Levels

Intracellular ROS levels were measured using a DCFH-DA probe (Beyotime, Shanghai, China, S0033S). Briefly, 5×10^3 cells were seeded into 96-well plates and incubated with 8 μM DCFH-DA at 37 °C for 15 min. The results were observed under a fluorescence microscope.

2.18 Statistical Analysis

GraphPad Prism 9.0.0 (GraphPad Software, Boston, MA, USA) was utilized for carrying out statistical analysis and data visualization. Data were expressed as mean ± standard deviation. A *t*-test was applied for making comparisons between groups, with $p < 0.05$ denoting a statistically significant difference. All animal experiments were each conducted with six biological replicates, and all cell experiments were each carried out with three biological replicates.

3. Results

3.1 Screening of DEGs

Differential expression analysis was performed on the GSE193677 dataset using the thresholds of $|\log_2 FC| > 1$ & adj. *p* value < 0.05. A total of 516 DEGs were identified, comprising 84 downregulated and 432 upregulated genes (Fig. 1A,B). Functional enrichment analysis of these DEGs was subsequently conducted. In the GO-biological process (BP) category (Fig. 2A), DEGs were predominantly enriched in processes such as defense response to bacteria and humoral immune response. For the GO-cellular component (CC) category (Fig. 2B), enrichment of DEGs was observed in the immunoglobulin complex and the circulating immunoglobulin complex. In the GO-molecular function (MF) category (Fig. 2C), DEGs were mainly associated with antigen binding, immunoglobulin receptor binding, and cytokine activity. KEGG pathway analysis (Fig. 2D) revealed that these DEGs were principally enriched in the cytokine-cytokine receptor interaction pathway.
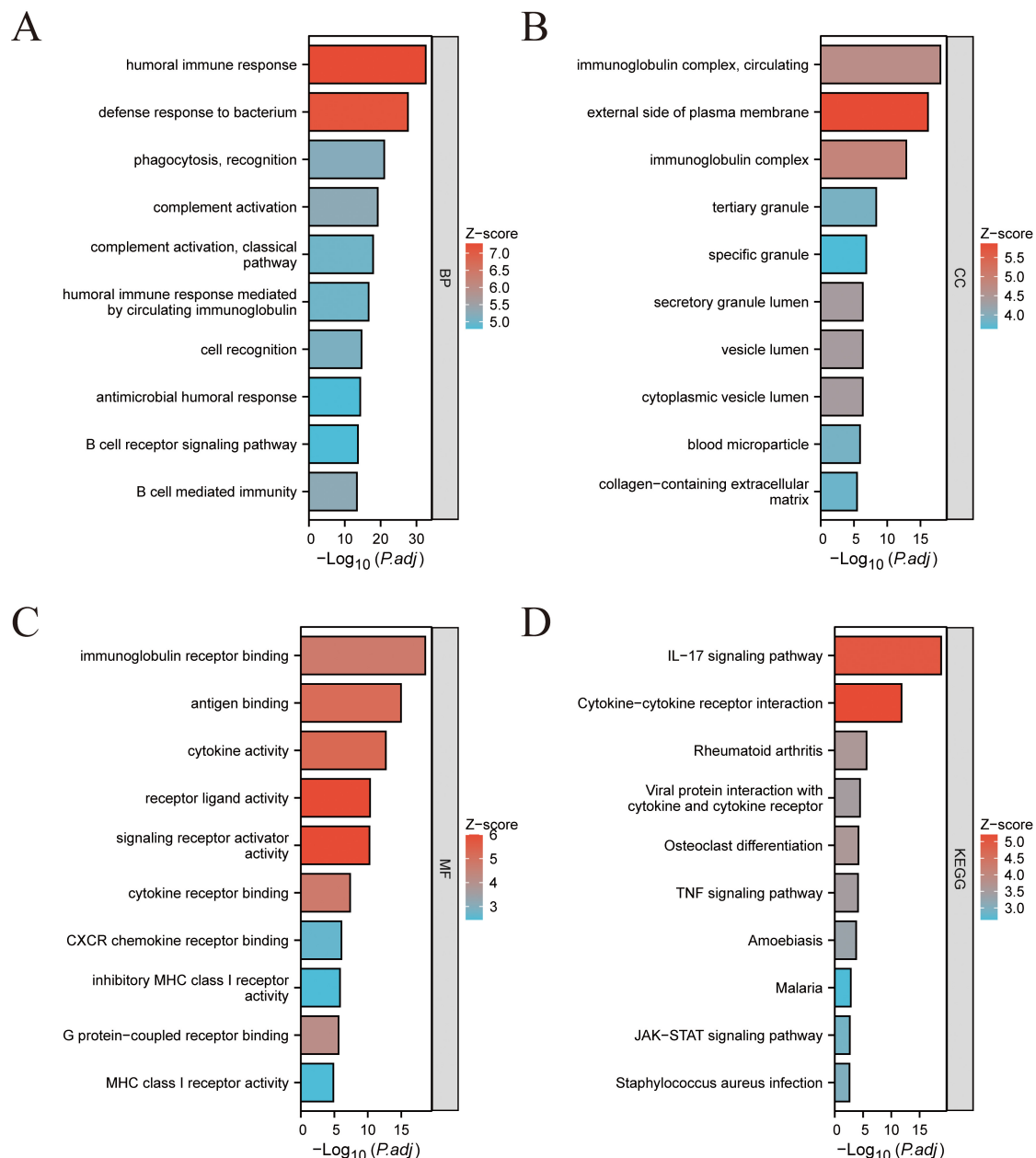
Fig. 2. Functional enrichment analysis of the identified DEGs. (A) GO-BP. (B) GO-CC. (C) GO-MF. (D) KEGG pathway enrichment analysis results. GO, gene ontology; BP, biological process; CC, cell component; MF, molecular function; KEGG, kyoto encyclopedia of genes and genomes.

3.2 Pyroptosis Score

Differential expression analysis was conducted on pyroptosis-related genes within the GSE193677 dataset, with the results presented in Fig. 3A. Pyroptosis scores for each sample were calculated via GSVA. The results demonstrated that the UC group exhibited elevated pyroptosis scores compared with the Control group (Fig. 3B).

3.3 Weighted Gene Co-Expression Network Analysis (WGCNA)

WGCNA was performed on the identified DEGs. Initial sample clustering led to the exclusion of four outlier samples (Fig. 4A), after which the remaining samples were re-clustered and a heatmap of clinical features was generated (Fig. 4B). Based on the scale-free topology criterion, a soft-thresholding power of 7 was selected to construct the weighted co-expression network (Fig. 4C–E). A topological overlap matrix (TOM) was then constructed (Fig. 4F), and inter-module correlations were analyzed (Fig. 4G). Through correlation analysis between clinical traits (pyroptosis score and UC status) and gene modules (Fig. 4H), two modules, blue (76 genes) and turquoise (252 genes), were identified with strong correlations ($p < 0.05$, r > 0.5). Gene significance (GS) and module membership (MM) analyses
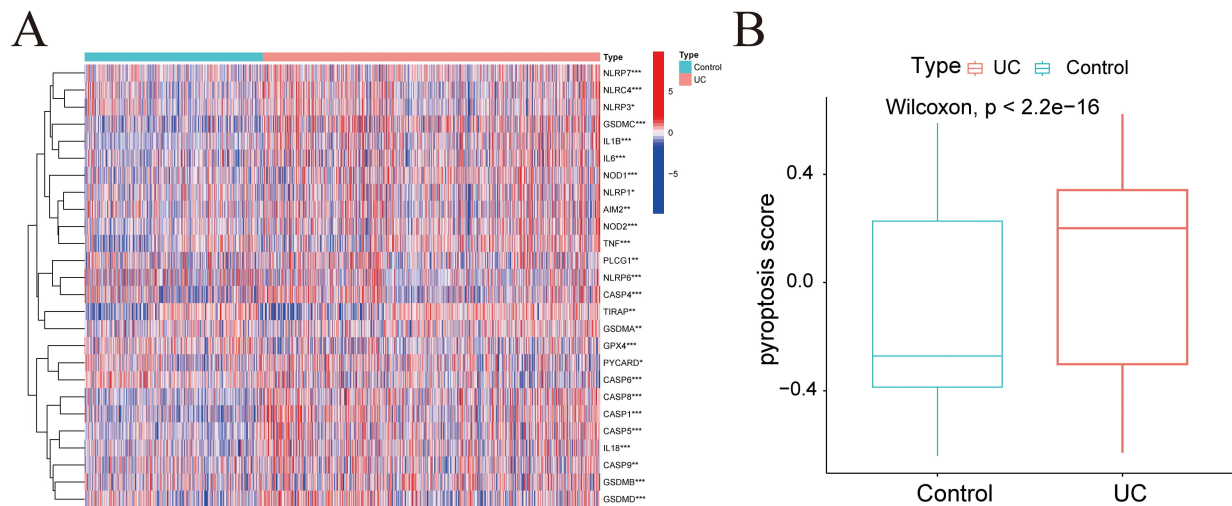
Fig. 3. Pyroptosis score. (A) Heatmap illustrating the expression of pyroptosis-related genes across samples from different groups in the GSE193677 dataset. (B) Bar chart showing the pyroptosis scores for each group. *$p < 0.05$; **$p < 0.01$; ***$p < 0.001$.
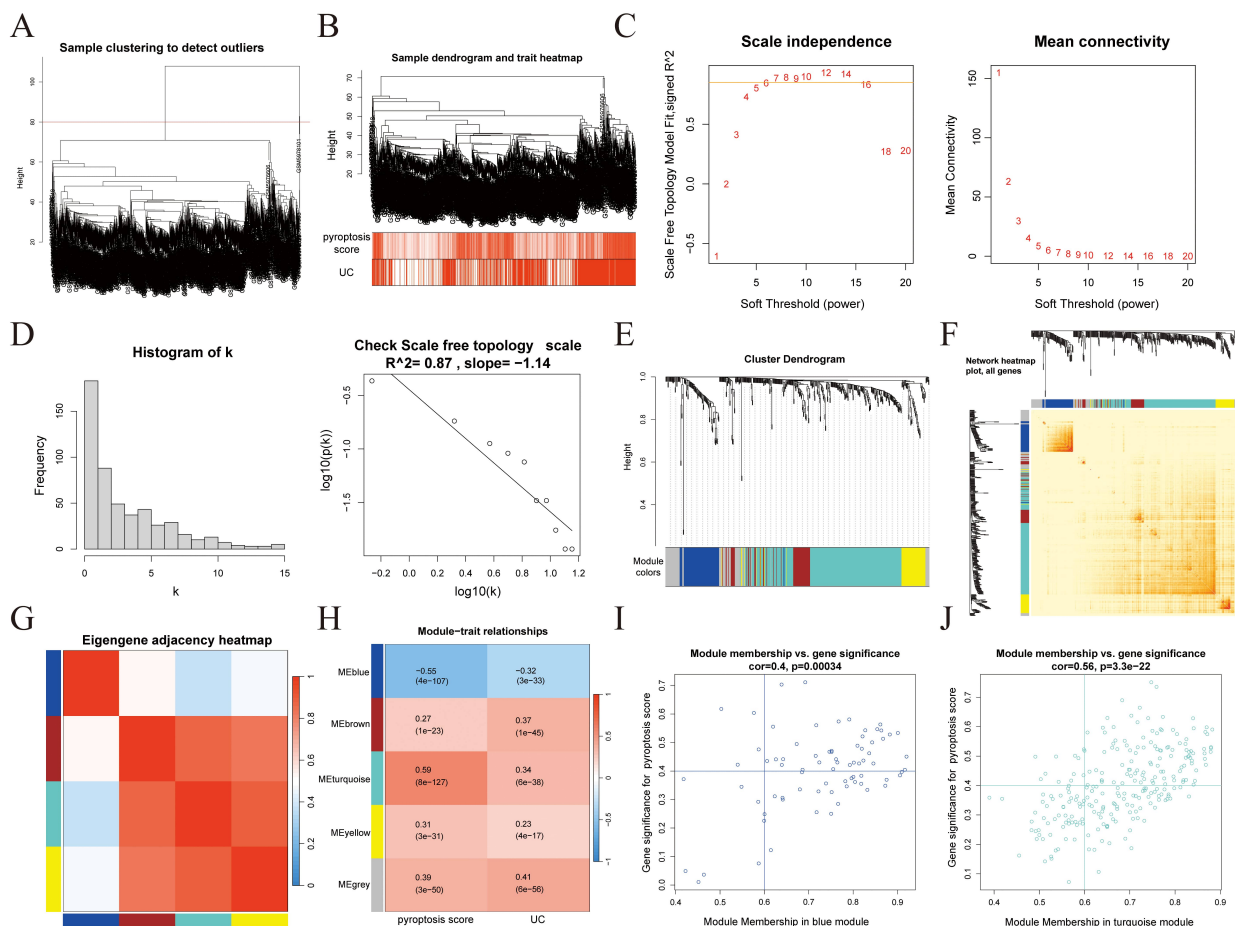

Fig. 4. WGCNA. (A) Sample clustering. (B) Sample clustering and clinical feature heatmaps. (C) Scale-free fitting index and average connectivity analysis under different soft threshold powers. (D) Visual testing of scale-free topologies. (E) Heatmap showing the correlation between module characteristic genes and clinical status. (F) TOM diagram. (G) Heatmap showing the correlation between modules. (H) Heatmap showing the correlation between modules and clinical features. (I) Correlation analysis of the blue module with UC. (J) Correlation analysis of the turquoise module with UC. WGCNA, weighted gene co-expression network analysis; TOM, topological overlap matrix; UC, ulcerative colitis.
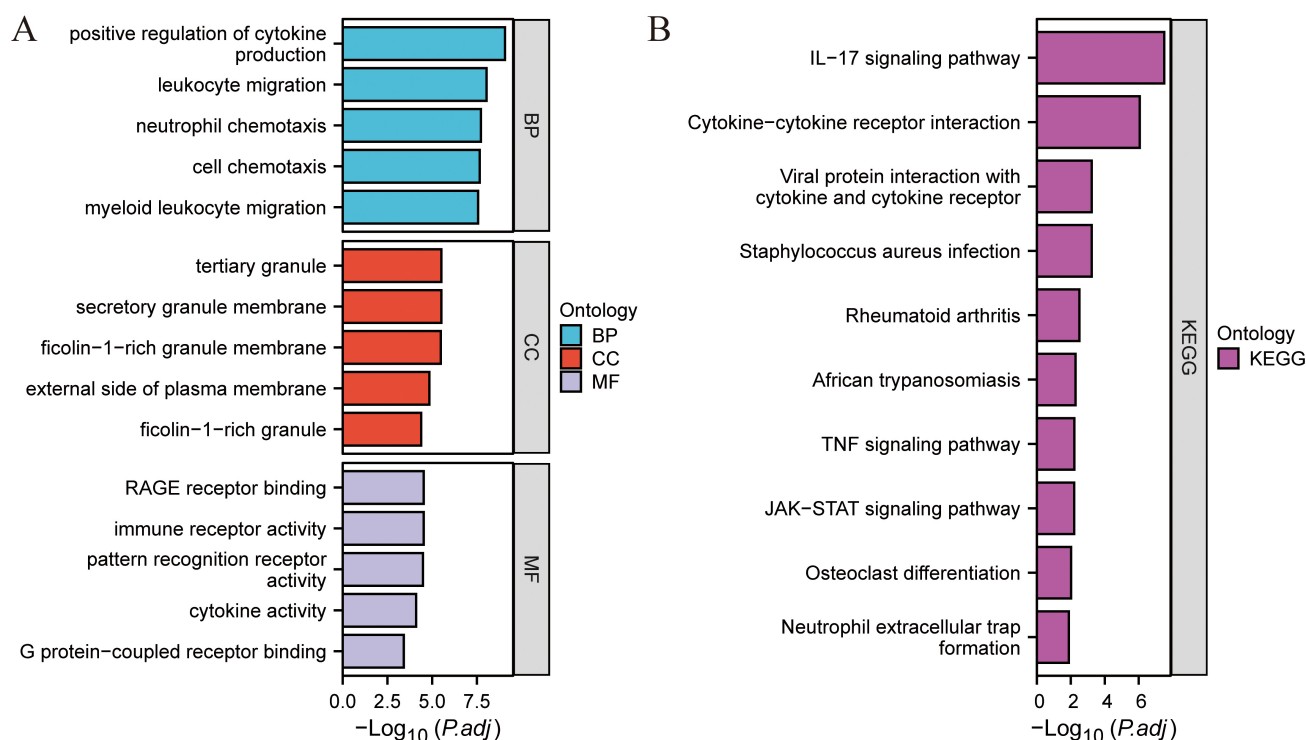
Fig. 5. Functional enrichment analysis. (A) GO enrichment. (B) KEGG pathway enrichment.

(Fig. 4I,J) confirmed that both modules were positively correlated with the pyroptosis score. A total of 149 key genes were subsequently identified using the criteria of MM >0.6 and GS >0.4, comprising 110 genes from the turquoise module and 39 from the blue module. Functional enrichment analysis of these key genes (Fig. 5A,B) revealed their predominant involvement in cytokine-cytokine receptor interaction, leukocyte migration, immune receptor activity, and positive regulation of cytokine production.

3.4 Hub Gene Screening

PPI analysis was conducted on the 149 key genes identified through WGCNA (Fig. 6A). Using Cytoscape, a core network comprising 12 genes (all upregulated in the UC group) was generated (Fig. 6B). Three machine learning algorithms were applied to these 12 genes to further identify hub genes: LASSO regression (Fig. 6C,D), random forest (Fig. 6E,F), and SVM-RFE (Fig. 6G). The intersection of results from all three algorithms yielded five hub genes: *AQP9*, *S100A8*, *S100A9*, *S100A12*, and *VNN2* (Fig. 6H).

3.5 Immunoinfiltration Analysis

Immunoinfiltration analysis was conducted on the GSE193677 dataset (Fig. 7A), and inter-correlations among immune cell populations were assessed (Fig. 7B). A strong positive correlation was revealed between neutrophils and Gamma delta T cells. The relative abundance of individual immune cell types was compared between the UC and Control groups (Fig. 7C), with statistically significant differences observed in 17 of 22 immune cell

types. Notably, AQP9 expression was positively correlated with neutrophils, macrophages M1, and plasma cells, while negatively correlated with resting mast cells, memory B cells, naïve CD4$^+$ T cells, resting dendritic cells, and macrophages M2 (Fig. 7D). These results suggest that AQP9 may modulate immune cell infiltration, thereby contributing to the pathogenesis of UC.

3.6 Correlation Between AQP9 and Pyroptosis

Correlation analysis revealed a significant association between AQP9 expression and pyroptosis scores (Fig. 8A). Consistently, AQP9 was upregulated in the UC group within the GSE193677 dataset (Fig. 8B). ssGSEA indicated that AQP9 may influence the JAK-STAT pathway (Fig. 8C). According to recent literature, the JAK-STAT pathway plays a pivotal role in the regulation of pyroptosis [13].

3.7 AQP9 is Predominantly Expressed in Neutrophils

We interrogated the single-cell RNA sequencing dataset GSE214695 to pinpoint the specific cell type in which AQP9 exerts its influence on the pathogenesis of UC. Upon clustering, a total of 24 distinct cell clusters were identified (Fig. 9A). These clusters were subsequently annotated into nine cell types: T cells, tissue stem cells, neutrophils, epithelial cells, macrophages, B cells, common myeloid progenitors, endothelial cells, and neurons (Fig. 9B). Differential expression analysis of AQP9 across these cell types revealed significant upregulation of AQP9 in epithelial cells and neutrophils, with no significant differ-
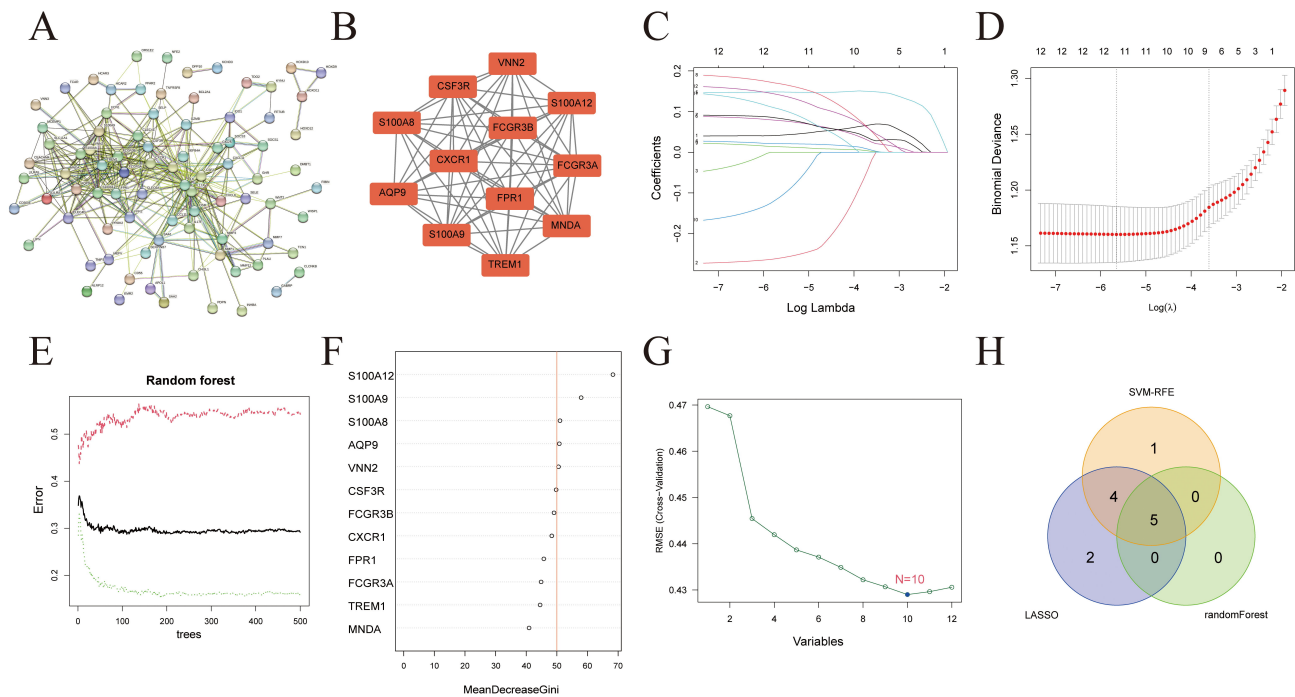
Fig. 6. Hub gene screening. (A) PPI network of 149 WGCNA-derived genes. (B) Key genes identified within the PPI network. (C) Calculation of regression coefficients. (D) Best forecasting models. (E) The effect of the decision tree number on error rate. (F) Results of the Gini coefficient method in a random forest classifier. (G) RMSE evaluates SVM regression models. (H) A Venn diagram illustrating the similarities and differences among the results of the three machine learning algorithms. PPI, protein-protein interaction; RMSE, root mean square error; SVM, support vector machine.

ential expression observed in B cells, T cells, endothelial, or macrophages and no expression in the remaining cell types (Fig. 9C). Therefore, AQP9 is predominantly expressed in neutrophils and, notably, its expression is elevated in neutrophils from UC patients compared to those from individuals in the Control group (Fig. 9C).
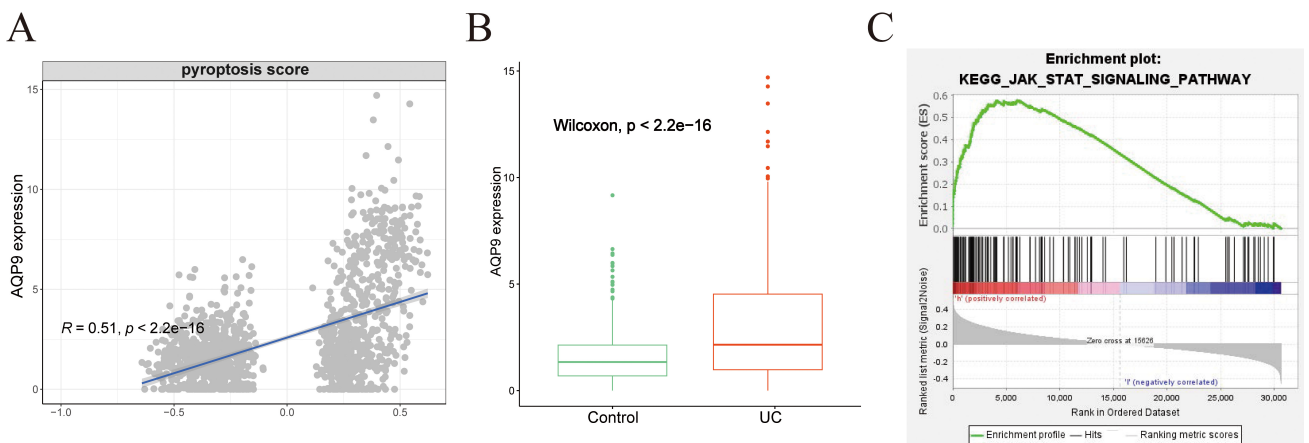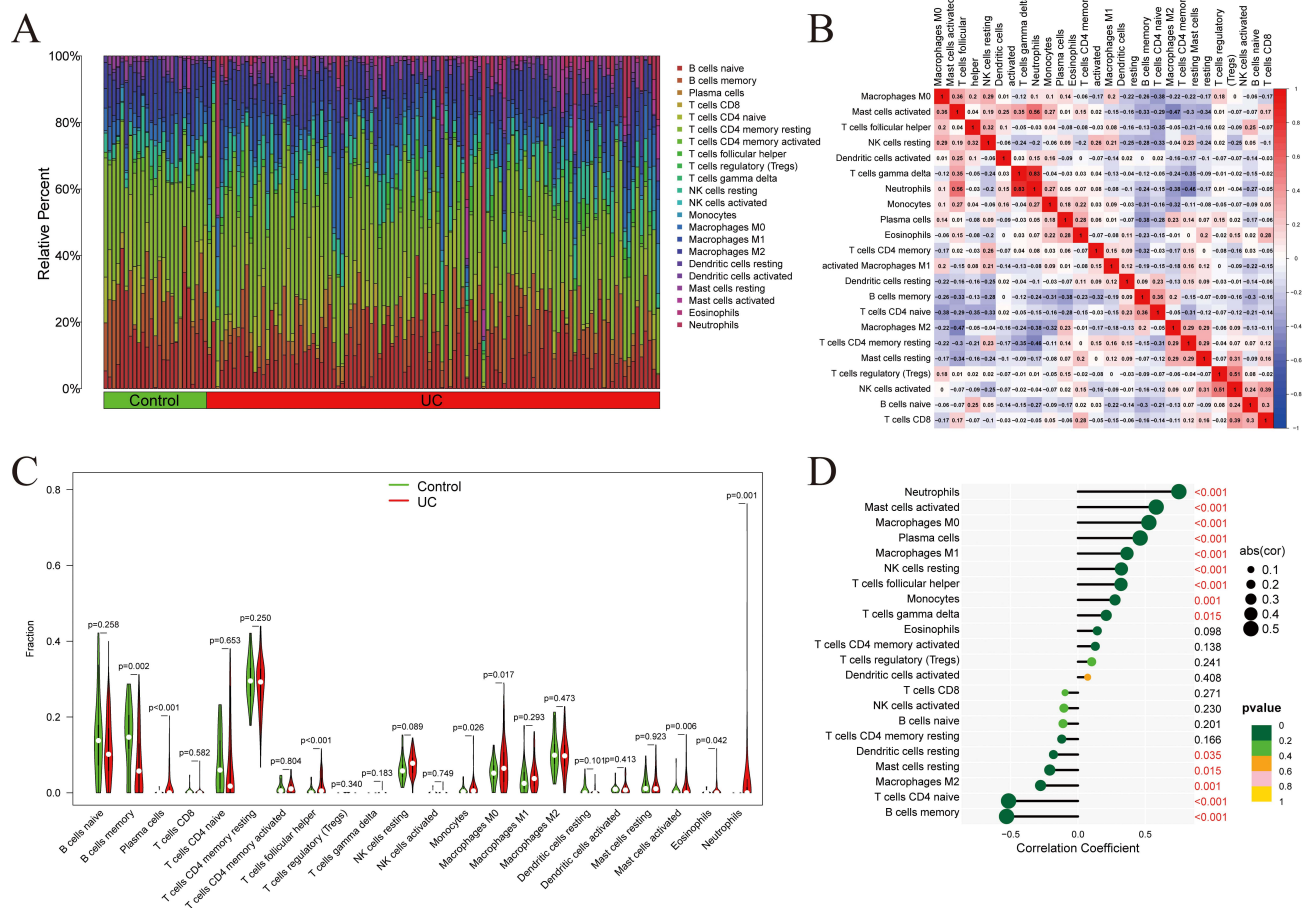
3.8 AQP9 is Highly Expressed in the Colon Tissues of Mice With UC

To validate findings from the bioinformatics analysis described above, a mouse model of UC was established. Mice in the Control group were maintained on a standard diet and water intake, and they exhibited normal activity and stable body weight. In contrast, mice in the UC group displayed reduced activity, curled postures, and significant body weight loss after 4–5 days of modeling (Fig. 10A). Additionally, the spleen index was elevated in the UC group compared to the Control group (Fig. 10B). Macroscopically, colon tissues from the Control group showed no signs of hemorrhage or ulceration, whereas those from the UC group exhibited marked intestinal congestion, hemorrhagic changes, and substantial colon shortening (Fig. 10C). Histological examination revealed that colonic architecture was preserved in the Control group, with intact glandular structures, well-aligned epithelial cells, normal crypt morphology, and preserved lamina propria and muscular layers. In contrast, the UC group demonstrated extensive inflamma-

tory cell infiltration, disrupted mucosal architecture, crypt loss, ulceration, and epithelial necrosis (Fig. 10D). Consistent with these pathological changes, the expression of pro-inflammatory cytokines IL-18 and IL-1β was significantly upregulated in the colon tissues of mice with UC (Fig. 10E), while that of ZO-1 and occludin were markedly downregulated (Fig. 10F). Subsequent WB and qRT-PCR analyses confirmed a significant upregulation of AQP9 expression in the UC group (Fig. 10F–H), consistent with the findings from bioinformatics analysis. Ly6G is a specific surface marker for neutrophils. In the merged immunofluorescence image, we observed significant overlap between the Ly6G and AQP9 signals, which is displayed as a yellow signal. This indicates that AQP9 is expressed in neutrophils (Fig. 10H). Moreover, the levels of NET-associated markers MPO and CitH3 were found to be elevated in the UC group compared to the Control group. Immunofluorescence analysis showed their co-localization within the web-like structures of NETs, which is a hallmark of NETs (Fig. 10I).

3.9 AQP9 Knockdown Inhibits PMA-Induced Formation of NETs to Alleviate Intestinal Epithelial Cell Injury

Neutrophils were treated with PMA *in vitro* to induce the formation of NETs. PMA stimulation was revealed to promote the expression of NETs markers peptidylarginine deiminase 4 (PAD4), CitH3, and MPO (Fig. 11A,C), the expression of pyroptosis marker GSDMD-N (Fig. 11A), as

Fig. 7. Immunoinfiltration analysis. (A) Proportions of 22 immune cells in the samples within the GSE193677 dataset. (B) Correlations between immune cells. (C) Comparison of the differences in immune cells between the Control and UC groups. (D) Lollipop plot showing the correlation between immune cells and AQP9 expression (In the lollipop plot, the color of the circles represents the statistical significance of the correlation between genes and immune cells).

Fig. 8. Correlation between AQP9 and pyroptosis. (A) Correlation between AQP9 expression and pyroptosis scores. (B) Boxplot showing the expression of AQP9 in both the UC and Control groups. (C) Association between AQP9 expression and JAK-STAT pathway activity assessed by ssGSEA. ssGSEA, single-sample gene set enrichment analysis.

well as the expression of p-JAK2 and p-STAT3 (Fig. 11B). Additionally, PMA treatment upregulated AQP9 expression (Fig. 11B), elevated ROS levels (Fig. 11D), and increased IL-1β, Lactate Dehydrogenase (LDH), and MPO-DNA complex levels (**Supplementary Fig. 1**). To determine the regulatory role of AQP9, AQP9 expression was
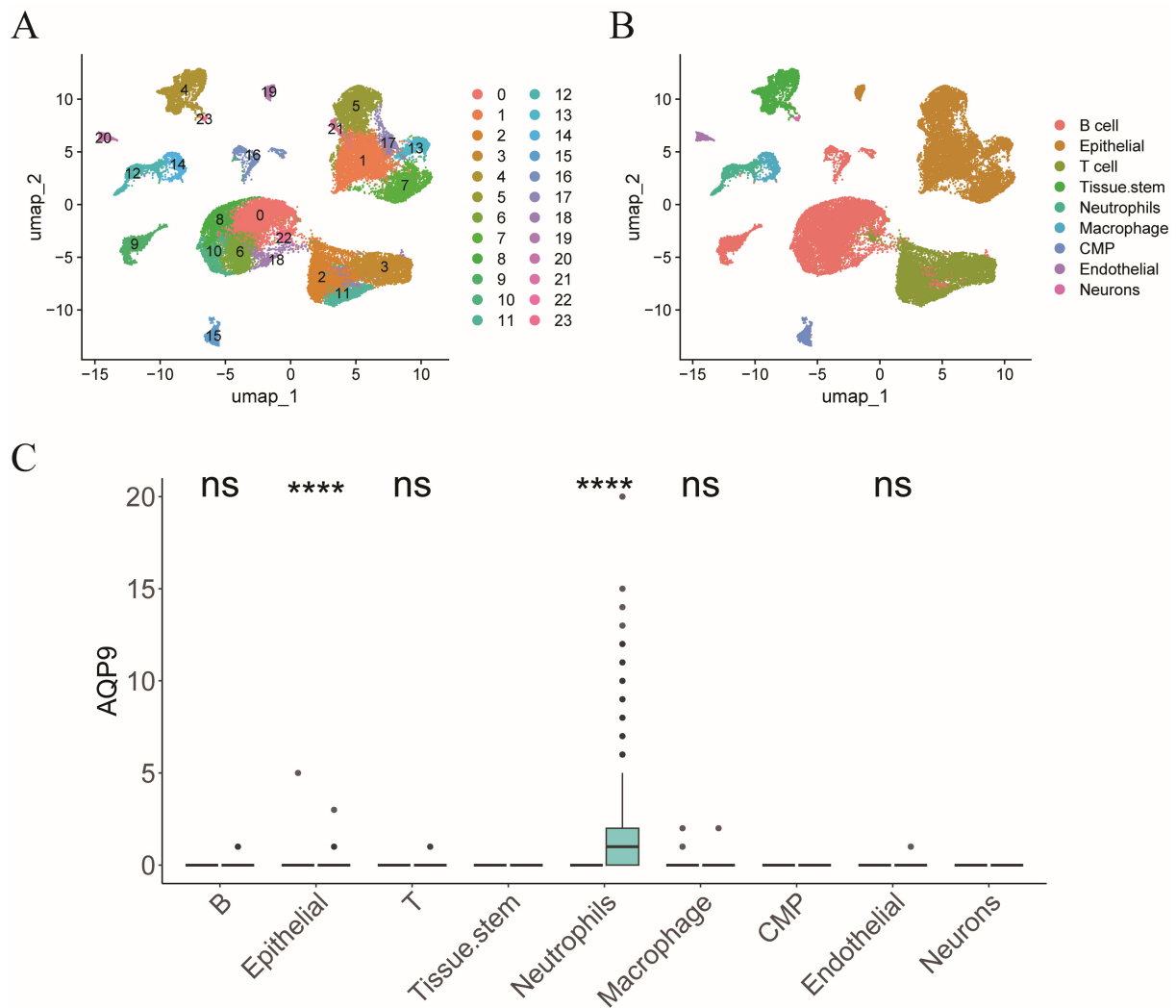
Fig. 9. AQP9 is predominantly expressed in neutrophils. (A) t-distributed stochastic neighbor embedding (t-SNE) plot showing cell clustering. (B) t-SNE plot illustrating cell annotation situation. (C) Bar chart displaying the differential expression of AQP9 in each cell across groups. CMP, common myeloid progenitors. $^{ns}p > 0.05$, $****p < 0.0001$.

silenced in the PMA-treated neutrophils. Knockdown of AQP9 significantly reduced the expression of PAD4, MPO, CitH3 (Fig. 11A,C), GSDMD-N (Fig. 11A), p-JAK2 and p-STAT3 (Fig. 11B), ROS levels (Fig. 11D), as well as levels of IL-1β, LDH, and MPO-DNA complex (**Supplementary Fig. 1**). Co-culture experiments with neutrophils and intestinal epithelial cells revealed that PMA treatment reduced epithelial cell viability (Fig. 11E), increased cell death (Fig. 11F), and suppressed the expression of ZO-1 and occludin (Fig. 11G). Conversely, AQP9 knockdown restored epithelial cell viability, decreased cell death, and promoted the expression of ZO-1 and occludin (Fig. 11E–G).

3.10 AQP9 Knockdown Inhibits Pyroptosis-Mediated Formation of NETs to Alleviate Intestinal Epithelial Cell Injury

To further elucidate the interplay between AQP9, pyroptosis, and the formation of NETs, neutrophils from the PMA+si-AQP9 group were treated with the pyroptosis ag-

onist Nigericin. Nigericin treatment did not alter AQP9 expression (Fig. 12A), but significantly enhanced GSDMD-N expression (Fig. 12B), upregulated the expression of NETs markers PAD4, MPO, and CitH3 (Fig. 12B,C), elevated ROS levels (Fig. 12D), and increased the levels of IL-1β, LDH, and MPO-DNA complex (**Supplementary Fig. 2**). Subsequent co-culture with intestinal epithelial cells demonstrated that, compared to the PMA+si-AQP9+EC group, the PMA+si-AQP9+Nigericin+EC group exhibited reduced epithelial cell viability (Fig. 12E), increased cell death (Fig. 12F), and decreased expression of ZO-1 and occludin (Fig. 12G).

3.11 AQP9 Knockdown Regulates Pyroptosis-Mediated Formation of NETs by Inhibiting the JAK2-STAT3 Pathway to Alleviate Intestinal Epithelial Cell Injury

Based on the results from our previous experiments showing that AQP9 knockdown suppresses the JAK2-STAT3 pathway (Fig. 11B), we hypothesized that AQP9
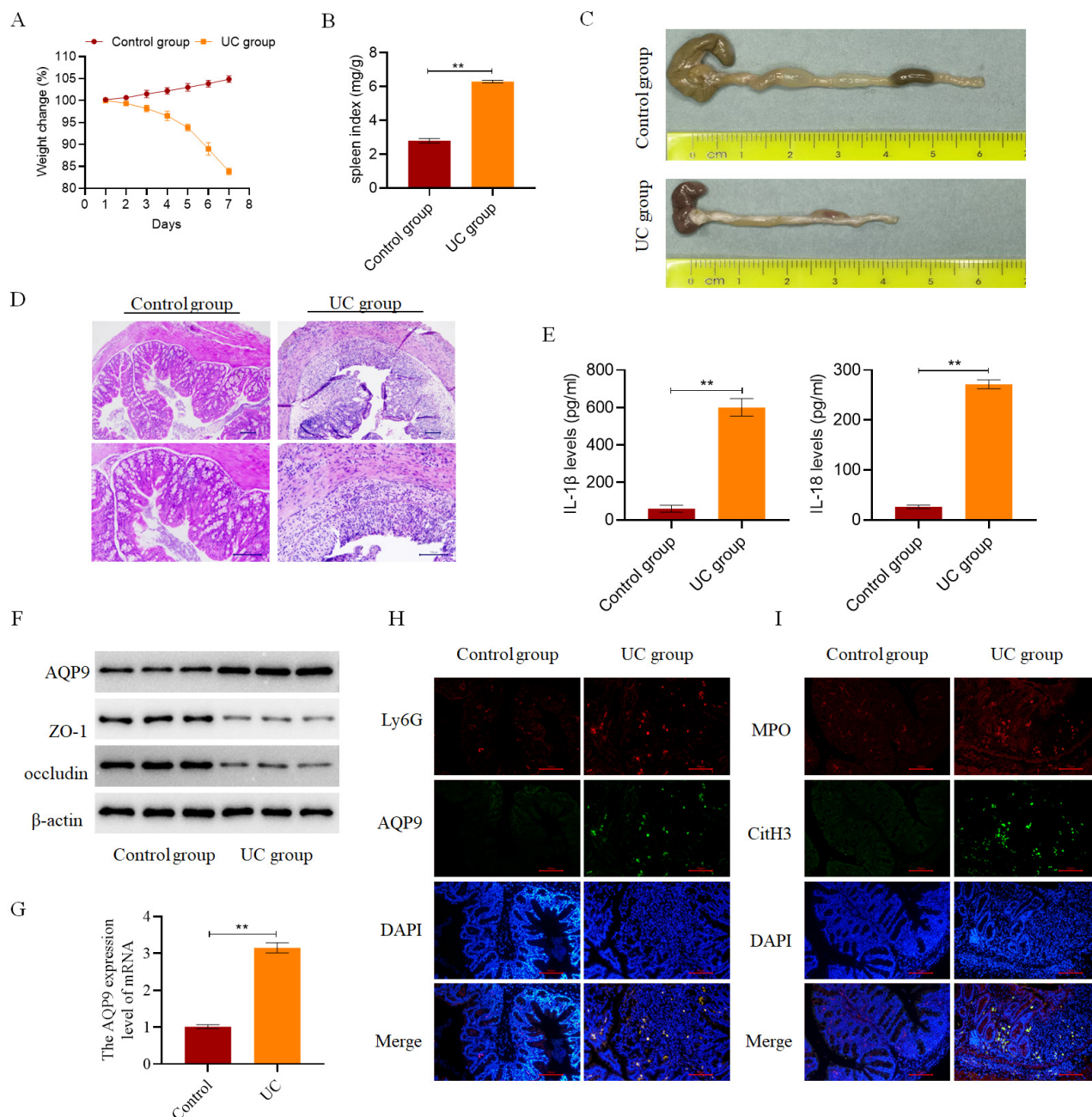
Fig. 10. AQP9 is highly expressed in the colon tissues of mice with UC. (A) Daily body weight changes of mice in both the Control and UC groups (n = 6). (B) Spleen index was measured in mice from both the Control and UC groups on day 7 post-modeling (n = 6). (C) Colon length was measured in mice from both the Control and UC groups on day 7 post-modeling (n = 6). (D) Histopathological changes in mouse colon tissue were examined in both the Control and UC groups on day 7 post-modeling (n = 6, scale bar = 100 μm). (E) Measurement of the levels of IL-18 and IL-1β in mouse colon tissues by ELISA in both the Control and UC groups on day 7 post-modeling (n = 6). (F) Detection of the expression of AQP9 and pyroptosis-related proteins in mouse colon tissues by WB in both the Control and UC groups on day 7 post-modeling (n = 6). (G) Detection of the expression of AQP9 in mouse colon tissue by qRT-PCR in both the Control and UC groups on day 7 post-modeling (n = 6). (H) Assessment of the expression of AQP9 and Ly6G in mouse colon tissue by immunofluorescence in both the Control and UC groups on day 7 post-modeling (n = 6, scale bar = 100 μm). (I) Assessment of the expression of MPO and CitH3 in mouse colon tissue by immunofluorescence in both the Control and UC groups on day 7 post-modeling (n = 6, scale bar = 100 μm). **$p < 0.01$. IL, interleukin; ELISA, enzyme linked immunosorbent assay; WB, western blotting; Ly6G, lymphocyte antigen 6 complex locus G6D; MPO, myeloperoxidase; CitH3, citrullinated histone H3.
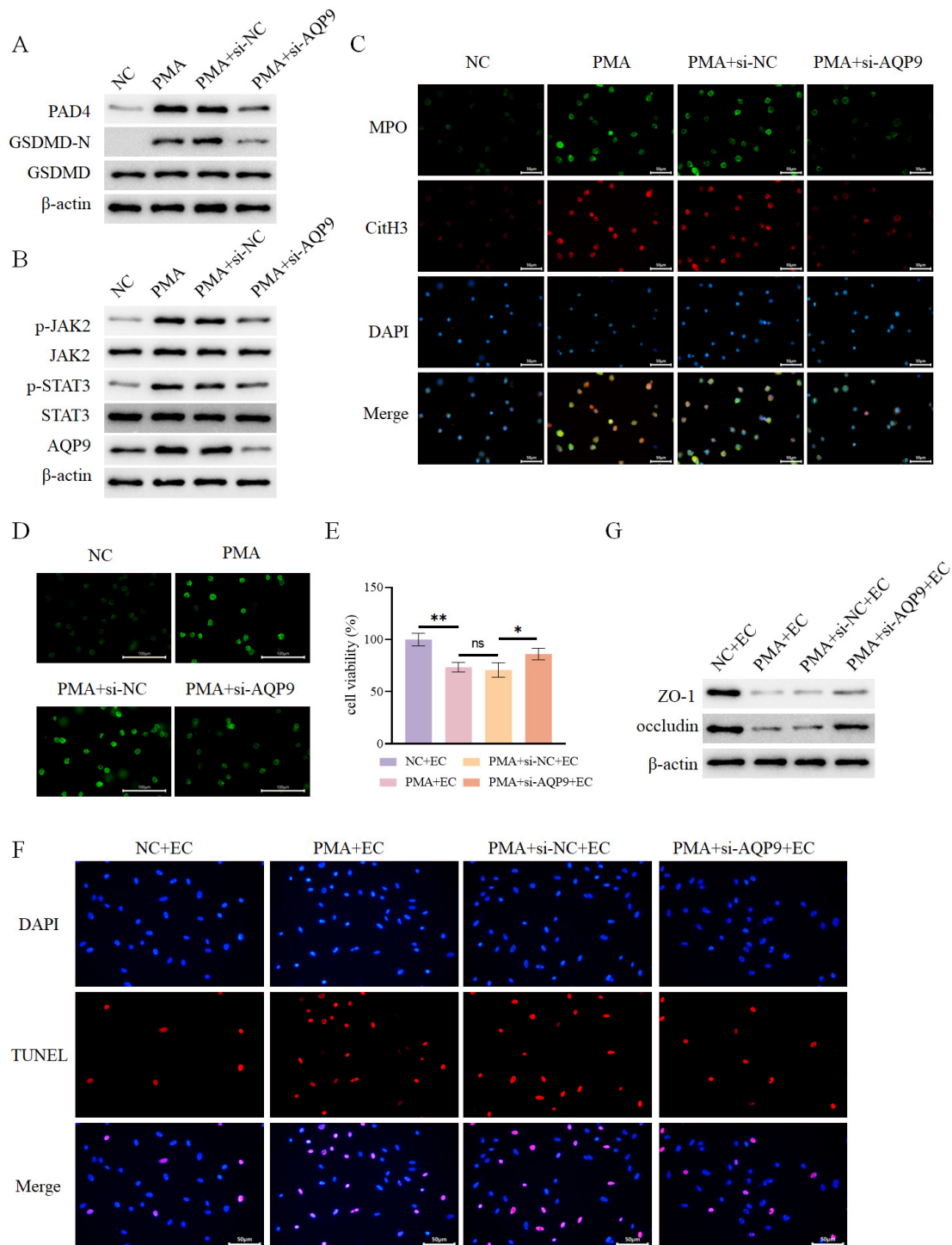
Fig. 11. AQP9 knockdown inhibits PMA-induced formation of NETs to alleviate intestinal epithelial cell injury. (A) Detection of intracellular expression of PAD4, GSDMD-N, and GSDMD in different groups by WB (n = 3). (B) Detection of intracellular expression of AQP9 and JAK2-STAT3 pathway-related proteins in different groups by WB (n = 3). (C) Assessment of intracellular expression of MPO and CitH3 in different groups by immunofluorescence (n = 3, scale bar = 50 μm). (D) Determination of intracellular ROS levels in different groups using a fluorescent probe (n = 3, scale bar = 100 μm). (E) Assessment of intestinal epithelial cell viability in each group after co-culture with the aforementioned neutrophils using the CCK-8 assay (n = 3). (F) Evaluation of intestinal epithelial cell death in each group by TUNEL assay (n = 3, scale bar = 50 μm). (G) Determination of the expression of ZO-1 and occludin in intestinal epithelial cells from each group by WB (n = 3). $^{ns}p > 0.05$; $^{*}p < 0.05$; $^{**}p < 0.01$. NETs, neutrophil extracellular traps; PAD4, peptidylarginine deiminase 4 ; GSDMD-N, cleaved N-terminal gasdermin D; ROS, reactive oxygen species; CCK-8, cell counting kit-8; TUNEL, terminal deoxynucleotidyl transferase dUTP nick end labeling; ZO-1, zonula occludens 1.
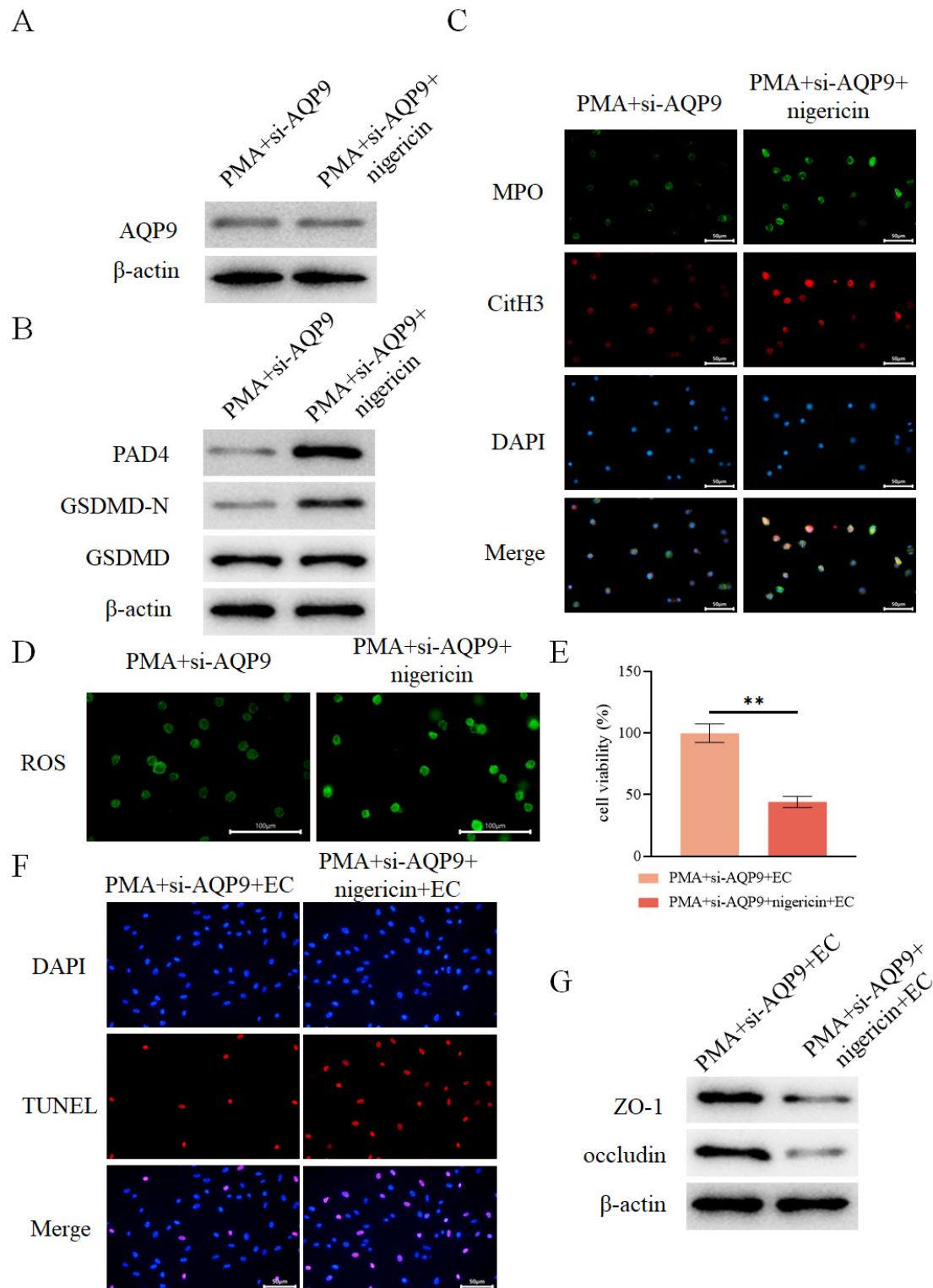
Fig. 12. AQP9 knockdown inhibits pyroptosis-mediated formation of NETs to alleviate intestinal epithelial cell injury. (A) Detection of intracellular AQP9 expression in different groups by WB (n = 3). (B) Detection of intracellular expression of PAD4, GSDMD-N, and GSDMD in different groups by WB (n = 3). (C) Assessment of intracellular expression of MPO and CitH3 in different groups by immunofluorescence (n = 3, scale bar = 50 μm). (D) Measurement of intracellular levels of ROS in different groups using a fluorescent probe (n = 3, scale bar = 100 μm). (E) Assessment of intestinal epithelial cell viability in each group after co-culture with the aforementioned neutrophils using the CCK-8 assay (n = 3). (F) Evaluation of intestinal epithelial cell death in each group by TUNEL assay (n = 3, scale bar = 50 μm). (G) Determination of the expression of ZO-1 and occludin in intestinal epithelial cells from each group by WB (n = 3). **$p < 0.01$.
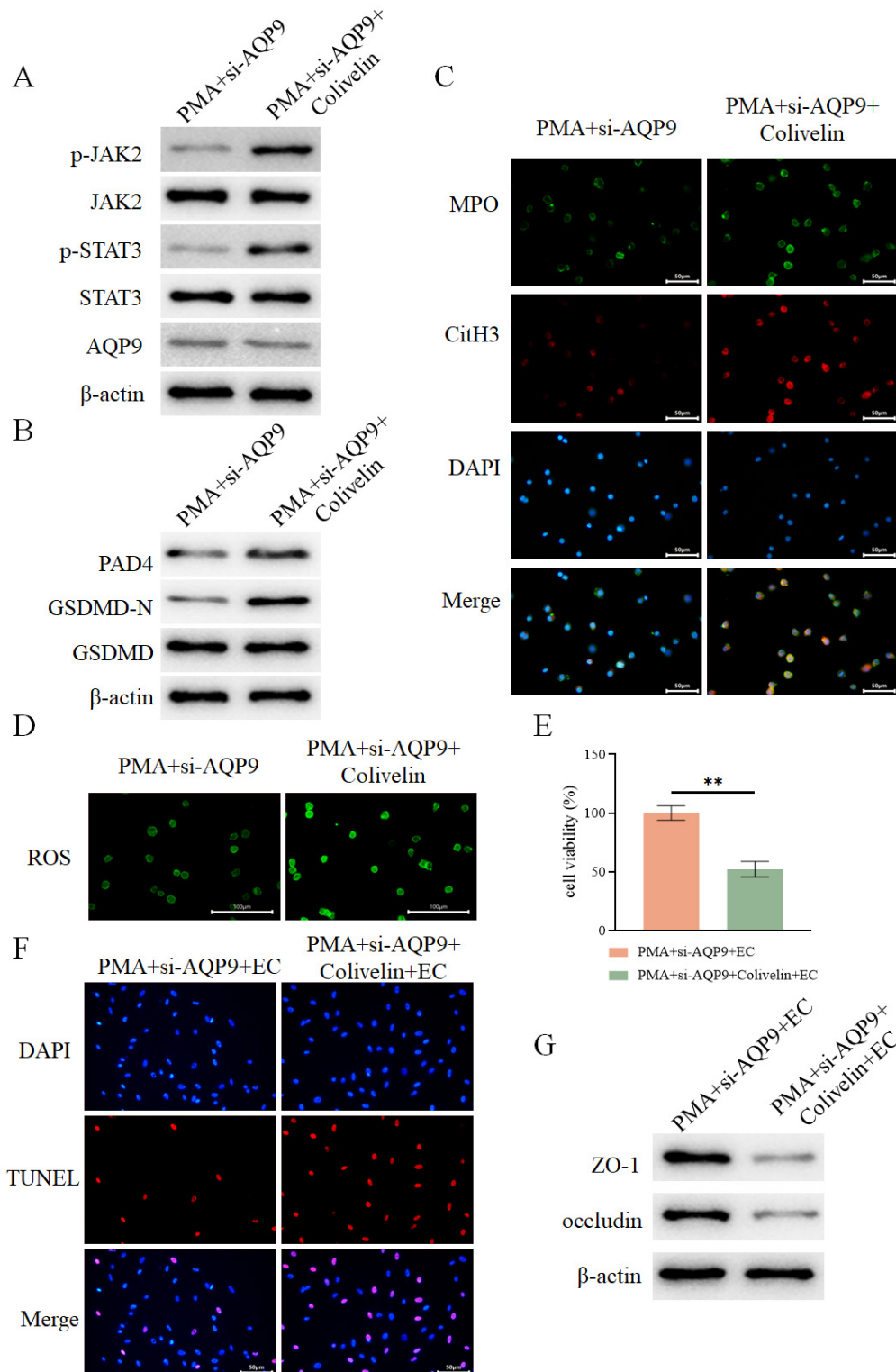
Fig. 13. AQP9 knockdown inhibits the JAK2-STAT3 pathway to regulate pyroptosis-mediated formation of NETs to alleviate intestinal epithelial cell injury. (A) Detection of intracellular expression of AQP9 and JAK2-STAT3 pathway-related proteins in different groups by WB (n = 3). (B) Detection of intracellular expression of PAD4, GSDMD-N, and GSDMD in different groups by WB (n = 3). (C) Assessment of intracellular expression of MPO and CitH3 in different groups by immunofluorescence (n = 3, scale bar = 50 µm). (D) Measurement of intracellular ROS levels in different groups using a fluorescent probe (n = 3, scale bar = 100 µm). (E) Assessment of intestinal epithelial cell viability in each group after co-culture with the aforementioned neutrophils using the CCK-8 assay (n = 3). (F) Evaluation of intestinal epithelial cell death in each group by TUNEL assay (n = 3, scale bar = 50 µm). (G) Determination of the expression of ZO-1 and occludin in intestinal epithelial cells from each group by WB (n = 3). **$p < 0.01$.

may regulate pyroptosis via modulation of this pathway. To make further validation, neutrophils from the PMA+si-AQP9 group were treated with the JAK2-STAT3 pathway agonist Colivelin. It was revealed that treatment with Colivelin did not affect AQP9 expression (Fig. 13A) but markedly enhanced the expression of JAK2, STAT3, and GSDMD-N (Fig. 13A,B). Additionally, the levels of NET-associated proteins PAD4, MPO, and CitH3 were upregulated (Fig. 13B,C), ROS levels were elevated (Fig. 13D), and levels of IL-1β, LDH, and MPO-DNA complex were increased (**Supplementary Fig. 3**). Co-culture with epithelial cells demonstrated that Colivelin-treated neutrophils significantly inhibited epithelial cell viability (Fig. 13E), increased cell death (Fig. 13F), and downregulated ZO-1 and occludin expression (Fig. 13G), thereby reversing the protective effects conferred by AQP9 silencing.

4. Discussion

UC is clinically characterized by persistent or recurrent diarrhea, abdominal pain, and other systemic manifestations, posing considerable challenges for effective treatment [2]. The disease substantially reduces patients' quality of life and has a significant impact on patients' mental health [14]. In the present study, 516 DEGs were screened out from UC-related datasets. Functional enrichment analysis revealed that these DEGs were predominantly associated with immunoglobulin receptor binding, humoral immune responses, circulating immunoglobulin complexes, antigen binding, defense responses to bacterial pathogens, cytokine activity, and cytokine-cytokine receptor interactions. Aberrant immune responses involving the gut microbiota are widely recognized as central to the pathogenesis of IBD [15]. Previous study have demonstrated that the damage-related protein high mobility group box 1 protein (HMGB1) in intestinal epithelial cells can regulate autophagy through STAT3, thereby protecting the intestine from bacterial infection and damage [16]. Additionally, lactate has been reported to regulate macrophage polarization both *in vitro* and *in vivo*, inhibit the production of pro-inflammatory cytokines, and modulate the intestinal microbiota to attenuate DSS-induced colitis in murine models [17]. Moreover, the combination of ziyuglycoside II, syringin, and pedunculoside has been reported to suppress cytokine-cytokine receptor interaction pathways and maintain the integrity of the intestinal mucosal barrier, thereby influencing the progression of UC [18].

Pyroptosis is a known form of programmed cell death. Its inhibition has emerged as a promising therapeutic strategy to slow the progression of UC. Study have reported that engineered lactic acid-producing probiotic yeasts can inhibit macrophage pyroptosis, regulate gut microbiota composition, and mitigate mucosal damage in animal models. This intervention enhances the mucosal barrier and dampens intestinal immune responses, thereby effectively delaying disease progression [17]. In addition, salidroside has

been shown to attenuate UC by inhibiting macrophage pyroptosis [19], while Shen-Ling-Bai-Zhu-San has shown the potential to improve DSS-induced colitis by suppressing caspase-1/caspase-11-mediated pyroptosis of colonic mucosal epithelial cells [20]. Based on these findings, our study aimed to identify key molecular factors associated with pyroptosis that may influence UC progression. Pyroptosis scores were calculated for each sample, revealing a significant difference between UC patients and healthy controls. Subsequently, WGCNA was performed on the identified DEGs to identify gene modules significantly correlated with pyroptosis and UC. To further screen core genes within the key modules, PPI network analysis and three distinct machine learning algorithms were employed, leading to the identification of five hub genes: *AQP9*, *S100A8*, *S100A9*, *S100A12*, and *VNN2*.

AQP9 is a water-selective membrane channel that has been documented in various diseases, including hepatitis [21], clear cell renal cell carcinoma [22], lung cancer [23], and acute myelogenous leukemia [24]. In colon cancer, AQP9 participates in lactate transport within tumor-associated macrophages and influences macrophage polarization [25]. Moreover, AQP9 functions as an immune-related prognostic biomarker, regulating the migration, proliferation, and invasion of laryngeal cancer cells [26] and hepatocellular carcinoma cells [27]. Based on single-cell transcriptomic analysis and immunofluorescence validation, it is hypothesized that AQP9 may play a regulatory role in neutrophils in the context of UC. Notably, study addressing the interplay between neutrophils and pyroptosis in UC remain limited. Therefore, the present study sought to further investigate the role of AQP9 in modulating UC progression via neutrophil-mediated mechanisms.

GSEA revealed that AQP9 may regulate the JAK-STAT pathway, a pathway crucial for various important biological processes. As reported, the JAK-STAT pathway plays a pivotal role in the pathogenesis of various diseases. JAK inhibitors have been approved for the treatment of multiple autoimmune conditions, including UC [28], rheumatoid arthritis, psoriasis, and atopic dermatitis [29]. Notably, a polypeptide (*Moringa oleifera* Lam. Peptide) isolated from oil sunflower seeds was demonstrated to reshape the intestinal mucosal barrier by inhibiting activation of the JAK-STAT pathway and regulating the gut microbiota, thereby improving UC [30]. Similarly, preclinical study demonstrated that Sishen Pill, a classical Chinese medicinal formulation, exerts therapeutic effects on UC. Its mechanism involves restoring immune homeostasis mediated by memory follicular T cells and memory T cells through suppression of the JAK/STAT pathway [31]. In Drosophila, ursolic acid was found to attenuate SDS-induced intestinal injury via inhibition of the JNK/JAK/STAT pathway, thereby exerting protective effects against UC [32]. In the present study, silencing AQP9 inhibited activation of the JAK2-STAT3 pathway,

thereby suppressing neutrophil pyroptosis and the formation of NETs. Consistently, in models of acute kidney injury, dimethyl fumarate was shown to mitigate pyroptosis in HK-2 renal epithelial cells through inhibition of the JAK2-STAT3 signaling axis [13]. Moreover, guanylate binding protein 5 (GBP5) induces classical pyroptosis in ovarian cancer cells via the JAK2/STAT1 pathway, thereby inhibiting tumor progression [33]. While existing studies have demonstrated that NETs can target the secretion of pro-inflammatory cytokines through the JAK/STAT pathway, the regulation of NETs by the JAK/STAT pathway remains unexplored. To clarify that the JAK2-STAT3 pathway can regulate pyroptosis of neutrophils, we treated neutrophils from the PMA+si-AQP9 group with JAK2-STAT3 pathway agonists and observed enhanced pyroptosis of neutrophils and the formation of NETs.

Kanako Watanabe-Kusunoki *et al*. [34] reported that GSDMD regulates neutrophil maturation and subsequent necrosis, and that the formation of NETs is reduced in GSDMD$^{-/-}$ mice in the context of thrombotic microangiopathy. Likewise, Huang *et al*. [35] demonstrated that ficolin-A aggravates the formation of NETs through GSDMD in LPS-mediated lung injury. Furthermore, Weijie Chen *et al*. [36] showed in zebrafish that *Edwardsiella piscicida* induces the formation of NETs by regulating pyroptosis-related proteins caspase-B and GSDMEb. Collectively, the foregoing findings suggest a potential link between neutrophil pyroptosis and NET formation. To validate this hypothesis, neutrophils from the PMA+si-AQP9 group were treated with a pyroptosis agonist, which significantly enhanced NET formation. Our results indicate that AQP9 knockdown inhibits JAK2-STAT3-mediated pyroptosis and subsequently suppresses NET formation. Furthermore, co-culture experiments with treated neutrophils and intestinal epithelial cells revealed that silencing AQP9 attenuates epithelial cell injury by inhibiting JAK2-STAT3-mediated pyroptosis and NET formation, highlighting a potential therapeutic strategy for preserving intestinal barrier function in UC.

5. Conclusions

In this study, AQP9 was identified through bioinformatics analysis as a key gene related to neutrophil pyroptosis and the progression of UC. Subsequent animal and cell experiments confirmed that AQP9 knockdown inhibits pyroptosis mediated by the JAK2-STAT3 pathway to suppress the formation of NETs, thereby alleviating intestinal epithelial cell injury. According to our findings, AQP9 can function as a potential target for regulating the formation of NETs, which offer novel insights into the mechanisms underlying the progression of UC. Nevertheless, certain limitations remain. While this study provides preliminary evidence that AQP9 may act as an upstream regulator of the JAK2-STAT3 pathway to modulate neutrophil pyroptosis and NET formation, the precise molecular mechanisms by which AQP9 regulates this pathway remain to be elucidated. Additionally, although we primarily investigated the role of AQP9 knockdown in NET formation, future studies involving AQP9 overexpression are necessary to conclusively establish its regulatory role in the JAK2-STAT3 pathway. Furthermore, the other four genes identified through bioinformatics analysis, *S100A8*, *S100A9*, *S100A12*, and *VNN2*, have not yet been experimentally investigated in the context of UC. Future studies should focus on elucidating their regulatory roles and underlying mechanisms in the pathogenesis of UC.

Abbreviations

UC, ulcerative colitis; NETs, neutrophil extracellular traps; IBD, inflammatory bowel disease; ROS, reactive oxygen species; GEO, gene expression omnibus; DEGs, differentially expressed genes; GSVA, gene set variation analysis; KEGG, kyoto encyclopedia of genes and genomes; GO, gene ontology; PPI, protein-protein interaction; ssGSEA, single-sample gene set enrichment analysis; HE, hematoxylin-eosin; CST, cell signaling technology; GO-BP, biological process; GO-CC, cellular component; GO-MF, molecular function; TOM, topological overlap matrix; GS, gene significance; MM, module membership; CMPs, common myeloid progenitors; DSS, dextran sulfate sodium salt; PMA, phorbol 12-myristate 13-acetate; AQP9, aquaporin 9; PAD4, peptidylarginine deiminase 4; ZO-1, zonula occludens 1; ELISA, enzyme-linked immunosorbent assay; CCK-8, cell counting kit-8; TUNEL, terminal deoxynucleotidyl transferase dUTP nick end labeling; SVM-RFE, support vector machine-recursive feature elimination; MPO, myeloperoxidase; CitH3, citrullinated histone H3; GSDMD-N, cleaved N-terminal gasdermin D; IL, interleukin; GAPDH, glyceraldehyde-3-phosphate dehydrogenase; RMSE, root mean square error; SVM, support vector machine; Ly6G, lymphocyte antigen 6 complex locus G6D; HMGB1, high mobility group box 1 protein; GBP5, guanylate binding protein 5.

Availability of Data and Materials

The datasets used and analysed during the current study are available from the corresponding author on reasonable request.

Author Contributions

ZW and YS originated the research conception, designed the study, performed formal analysis, and prepared the first draft of the manuscript. XZ and JS performed the experiments, analyzed the data, and prepared the figures and tables. LS provided both methodological and administrative support and was a major contributor in reviewing and editing the manuscript. All authors contributed to editorial changes in the manuscript. All authors read and approved the final manuscript. All authors have participated

IMR Press

sufficiently in the work and agreed to be accountable for all aspects of the work.

Ethics Approval and Consent to Participate

The animal experiment was approved by the Ethics Committee of Laboratory Animal Management and Welfare of the First Affiliated Hospital of Harbin Medical University (Approval No.: IACUC-2023053), and conducted following the ARRIVE guidelines.

Acknowledgment

Not applicable.

Conflict of Interest

The authors declare no conflict of interest.

Supplementary Material

Supplementary material associated with this article can be found, in the online version, at https://doi.org/10.31083/FBL46505.

References

[1] Rawat A, Srivastava R. Current Approaches to Ulcerative Colitis Management: A Comprehensive Overview of Methodologies and Treatments. Infectious Disorders Drug Targets. 2025; 25: e18715265315472. https://doi.org/10.2174/0118715265315472241029110236.

[2] You M, Li J, Wang X, Liu Y, Chen S, Wang P. Targeting SLC7 A11 Ameliorates Ulcerative Colitis by Promoting Efferocytosis Through the ERK1/2 Pathway. Inflammation. 2025. https://doi.org/10.1007/s10753-025-02312-6. (online ahead of print)

[3] Lamb CA, Kennedy NA, Raine T, Hendy PA, Smith PJ, Limdi JK, et al. British Society of Gastroenterology consensus guidelines on the management of inflammatory bowel disease in adults. Gut. 2019; 68: s1–s106. https://doi.org/10.1136/gutjnl-2019-318484.

[4] Adams SM, Close ED, Shreenath AP. Ulcerative Colitis: Rapid Evidence Review. American Family Physician. 2022; 105: 406–411.

[5] Zhang J, Lei H, Hu X, Dong W. Hesperetin ameliorates DSS-induced colitis by maintaining the epithelial barrier via blocking RIPK3/MLKL necroptosis signaling. European Journal of Pharmacology. 2020; 873: 172992. https://doi.org/10.1016/j.ejphar.2020.172992.

[6] Nakase H, Sato N, Mizuno N, Ikawa Y. The influence of cytokines on the complex pathology of ulcerative colitis. Autoimmunity Reviews. 2022; 21: 103017. https://doi.org/10.1016/j.autrev.2021.103017.

[7] Lu H, Lin J, Xu C, Sun M, Zuo K, Zhang X, et al. Cyclosporine modulates neutrophil functions via the SIRT6-HIF-1α-glycolysis axis to alleviate severe ulcerative colitis. Clinical and Translational Medicine. 2021; 11: e334. https://doi.org/10.1002/ctm2.334.

[8] Wei Q, Jiang H, Zeng J, Xu J, Zhang H, Xiao E, et al. Quercetin protected the gut barrier in ulcerative colitis by activating aryl hydrocarbon receptor. Phytomedicine. 2025; 140: 156633. https://doi.org/10.1016/j.phymed.2025.156633.

[9] Liu H, Sun J, Wang Z, Han R, Zhao Y, Lou Y, et al. S100a10 deficiency in neutrophils aggravates ulcerative colitis in mice. International Immunopharmacology. 2024; 128: 111499. https://doi.org/10.1016/j.intimp.2024.111499.

[10] Dinallo V, Marafini I, Di Fusco D, Laudisi F, Franzè E, Di Grazia A, et al. Neutrophil Extracellular Traps Sustain Inflammatory Signals in Ulcerative Colitis. Journal of Crohn's & Colitis. 2019; 13: 772–784. https://doi.org/10.1093/ecco-jcc/jjy215.

[11] Chen KW, Monteleone M, Boucher D, Sollberger G, Ramnath D, Condon ND, et al. Noncanonical inflammasome signaling elicits gasdermin D-dependent neutrophil extracellular traps. Science Immunology. 2018; 3: eaar6676. https://doi.org/10.1126/sciimmunol.aar6676.

[12] Ye Y, Dai Q, Qi H. A novel defined pyroptosis-related gene signature for predicting the prognosis of ovarian cancer. Cell Death Discovery. 2021; 7: 71. https://doi.org/10.1038/s41420-021-00451-x.

[13] An X, Yin M, Shen Y, Guo X, Xu Y, Cheng D, et al. Dimethyl fumarate ameliorated pyroptosis in contrast-induced acute renal injury by regulating endoplasmic reticulum stress and JAK2-STAT3 pathway. Renal Failure. 2025; 47: 2504633. https://doi.org/10.1080/0886022X.2025.2504633.

[14] Kózka M, Skowron W, Bodys-Cupak I. Determinants of the level of anxiety and fears in a group of patients with ulcerative colitis. Annals of Agricultural and Environmental Medicine. 2019; 26: 337–340. https://doi.org/10.26444/aaem/94651.

[15] Rengarajan S, Vivio EE, Parkes M, Peterson DA, Roberson EDO, Newberry RD, et al. Dynamic immunoglobulin responses to gut bacteria during inflammatory bowel disease. Gut Microbes. 2020; 11: 405–420. https://doi.org/10.1080/19490976.2019.1626683.

[16] Zhang YG, Zhu X, Lu R, Messer JS, Xia Y, Chang EB, et al. Intestinal epithelial HMGB1 inhibits bacterial infection via STAT3 regulation of autophagy. Autophagy. 2019; 15: 1935–1953. https://doi.org/10.1080/15548627.2019.1596485.

[17] Sun S, Xu X, Liang L, Wang X, Bai X, Zhu L, et al. Lactic Acid-Producing Probiotic Saccharomyces cerevisiae Attenuates Ulcerative Colitis via Suppressing Macrophage Pyroptosis and Modulating Gut Microbiota. Frontiers in Immunology. 2021; 12: 777665. https://doi.org/10.3389/fimmu.2021.777665.

[18] Li Y, Tian YY, Wang J, Lin R, Zhang Y, Zhang MM, et al. Main active components of Ilex rotunda Thunb. protect against ulcerative colitis by restoring the intestinal mucosal barrier and modulating the cytokine-cytokine interaction pathways. Journal of Ethnopharmacology. 2024; 318: 116961. https://doi.org/10.1016/j.jep.2023.116961.

[19] Liu X, Zhou M, Dai Z, Luo S, Shi Y, He Z, et al. Salidroside alleviates ulcerative colitis via inhibiting macrophage pyroptosis and repairing the dysbacteriosis-associated Th17/Treg imbalance. Phytotherapy Research. 2023; 37: 367–382. https://doi.org/10.1002/ptr.7636.

[20] Chao L, Li Z, Zhou J, Chen W, Li Y, Lv W, et al. Shen-Ling-Bai-Zhu-San Improves Dextran Sodium Sulfate-Induced Colitis by Inhibiting Caspase-1/Caspase-11-Mediated Pyroptosis. Frontiers in Pharmacology. 2020; 11: 814. https://doi.org/10.3389/fphar.2020.00814.

[21] Dutta A, Das M. Deciphering the role of aquaporins in metabolic diseases: A mini review. The American Journal of the Medical Sciences. 2022; 364: 148–162. https://doi.org/10.1016/j.amjms.2021.10.029.

[22] Xu WH, Shi SN, Xu Y, Wang J, Wang HK, Cao DL, et al. Prognostic implications of Aquaporin 9 expression in clear cell renal cell carcinoma. Journal of Translational Medicine. 2019; 17: 363. https://doi.org/10.1186/s12967-019-2113-y.

[23] Chen P, Li Q, Zhou Y, Lu H, Chen H, Qian M, *et al*. Clinical implication of aquaporin 9 in non-small cell lung cancer patients: its expression and relationship with clinical features and prognosis. Irish Journal of Medical Science. 2022; 191: 651–658. https://doi.org/10.1007/s11845-021-02523-4.

[24] Fu W, Zhu G, Xu L, Liu J, Han X, Wang J, *et al*. G-CSF upregulates the expression of aquaporin-9 through CEBPB to enhance the cytotoxic activity of arsenic trioxide to acute myeloid leukemia cells. Cancer Cell International. 2022; 22: 195. https://doi.org/10.1186/s12935-022-02613-y.

[25] Shi Y, Yasui M, Hara-Chikuma M. AQP9 transports lactate in tumor-associated macrophages to stimulate an M2-like polarization that promotes colon cancer progression. Biochem Biophys Rep. 2022; 31: 101317. https://doi.org/10.1016/j.bbrep.2022.101317.

[26] Ren L, Li P, Li Z, Chen Q. AQP9 and ZAP70 as immune-related prognostic biomarkers suppress proliferation, migration and invasion of laryngeal cancer cells. BMC Cancer. 2022; 22: 465. https://doi.org/10.1186/s12885-022-09458-8.

[27] Liao S, Chen H, Liu M, Gan L, Li C, Zhang W, *et al*. Aquaporin 9 inhibits growth and metastasis of hepatocellular carcinoma cells via Wnt/β-catenin pathway. Aging. 2020; 12: 1527–1544. https://doi.org/10.18632/aging.102698.

[28] Pérez-Jeldres T, Tyler CJ, Boyer JD, Karuppuchamy T, Yarur A, Giles DA, *et al*. Targeting Cytokine Signaling and Lymphocyte Traffic via Small Molecules in Inflammatory Bowel Disease: JAK Inhibitors and S1PR Agonists. Frontiers in Pharmacology. 2019; 10: 212. https://doi.org/10.3389/fphar.2019.00212.

[29] Philips RL, Wang Y, Cheon H, Kanno Y, Gadina M, Sartorelli V, *et al*. The JAK-STAT pathway at 30: Much learned, much more to do. Cell. 2022; 185: 3857–3876. https://doi.org/10.1016/j.cell.2022.09.023.

[30] Hong ZS, Xie J, Wang XF, Dai JJ, Mao JY, Bai YY, *et al*. *Moringa oleifera* Lam. Peptide Remodels Intestinal Mucosal Barrier by Inhibiting JAK-STAT Activation and Modulating Gut Microbiota in Colitis. Frontiers in Immunology. 2022; 13: 924178. https://doi.org/10.3389/fimmu.2022.924178.

[31] Wang M, Huang X, Kang Z, Huang J, Wei S, Zhao H, *et al*. Mechanism of Sishen-Pill-Regulated Special Memory T and mTfh Cell via Involving JAK/STAT5 Pathway in Colitis Mice. Evidence-Based Complementary and Alternative Medicine. 2022; 2022: 6446674. https://doi.org/10.1155/2022/6446674.

[32] Wei T, Wu L, Ji X, Gao Y, Xiao G. Ursolic Acid Protects Sodium Dodecyl Sulfate-Induced *Drosophila* Ulcerative Colitis Model by Inhibiting the JNK Signaling. Antioxidants. 2022; 11: 426. https://doi.org/10.3390/antiox11020426.

[33] Zou C, Shen J, Xu F, Ye Y, Wu Y, Xu S. Immunoreactive Microenvironment Modulator GBP5 Suppresses Ovarian Cancer Progression by Inducing Canonical Pyroptosis. Journal of Cancer. 2024; 15: 3510–3530. https://doi.org/10.7150/jca.94616.

[34] Watanabe-Kusunoki K, Li C, Bandeira Honda TS, Zhao D, Kusunoki Y, Ku J, *et al*. Gasdermin D drives focal crystalline thrombotic microangiopathy by accelerating immunothrombosis and necroinflammation. Blood. 2024; 144: 308–322. https://doi.org/10.1182/blood.2023021949.

[35] Huang L, Tan X, Xuan W, Luo Q, Xie L, Xi Y, *et al*. Ficolin-A/2 Aggravates Severe Lung Injury through Neutrophil Extracellular Traps Mediated by Gasdermin D-Induced Pyroptosis. The American Journal of Pathology. 2024; 194: 989–1006. https://doi.org/10.1016/j.ajpath.2024.02.011.

[36] Chen W, Zhao J, Mu D, Wang Z, Liu Q, Zhang Y, *et al*. Pyroptosis Mediates Neutrophil Extracellular Trap Formation during Bacterial Infection in Zebrafish. Journal of Immunology. 2021; 206: 1913–1922. https://doi.org/10.4049/jimmunol.2001335.